CMS Physics Analysis Summary

Contact: cms-pag-conveners-top@cern.ch 2016/03/18

Measurement of the differential cross section for $\mathrm{t\bar{t}}$ production in the dilepton final state at $\sqrt{s} = 13$ TeV

The CMS Collaboration

Abstract

Measurements of normalized differential top quark pair ($\mathrm{t\bar{t}}$) production cross sections in proton-proton collisions at a centre-of-mass energy of 13 TeV at the CERN LHC are presented. The data were recorded in 2015 with the CMS detector and correspond to an integrated luminosity of 2.2 fb^{-1}. The measurements are performed in the dilepton decay channels ($\mathrm{e^+e^-}$, $\mu^+\mu^-$, and $\mu^\pm\mathrm{e}^\mp$). The $\mathrm{t\bar{t}}$ production cross section is measured as a function of kinematics of the top quarks, the $\mathrm{t\bar{t}}$ system, and of the number of jets in the event. The results are compared with several perturbative QCD calculations and are found to be broadly in agreement with the predictions.

1 Introduction

Differential top quark pair ($t\bar{t}$) production cross sections have been measured at the CERN LHC at proton-proton (pp) centre-of-mass energies $\sqrt{s}$ = 7 and 8 TeV [1–5]. Similar measurements have been performed by the CMS Collaboration using a small fraction of the collision data recorded in 2015 at $\sqrt{s}$ = 13 TeV, corresponding to an integrated luminosity of 42 pb^{-1} [6, 7]. In this document, measurements of normalized differential $t\bar{t}$ production cross sections are presented using the complete 13 TeV data sample recorded in 2015, which corresponds to an integrated luminosity of 2.2 fb^{-1} [8]. This result complements the recent CMS measurements of the $t\bar{t}$ inclusive production cross section [9].

The measurements are performed in the dilepton channels, with two oppositely charged muons or electrons (e^+e^-, $\mu^+\mu^-$, $\mu^\pm e^\mp$) and at least two jets. The analysis follows, to a large extent, the methodology from previous CMS measurements at $\sqrt{s}$ = 8 TeV [3] and 13 TeV [6]. The $t\bar{t}$ differential cross section is determined as a function of the kinematics of the top quarks, $t\bar{t}$ system, and as a function of the number of jets in the event. The top quark and $t\bar{t}$ kinematics are estimated via a kinematic reconstruction algorithm [3, 6]. The normalized differential $t\bar{t}$ production cross section in a bin of a given observable is determined by counting the number of $t\bar{t}$ events in that bin, correcting for the detector effects and acceptance by means of a regularized unfolding procedure, and dividing by the total number of observed $t\bar{t}$ events in all bins of that observable.

The number of jets in the event is presented in a fiducial phase space defined by the kinematic requirements placed on the selected final-state objects. Thus the model dependence introduced by an extrapolation to an experimentally inaccessible phase space region is avoided. In order to facilitate the comparison with the state-of-the-art quantum chromodynamic (QCD) calculations, the top quark and $t\bar{t}$ distributions are determined at parton level and are extrapolated to the full phase space.

The results are compared to several theoretical predictions obtained with the generator MG5_aMC@NLO [10] interfaced with PYTHIA [11] for parton showering and hadronization, and the POWHEG [12–15] generator, interfaced to both PYTHIA and HERWIG++ [16].

Depending on the availablility of the theory predictions, the parton level results are compared to several perturbative QCD calculations beyond the next-to-leading-order (NLO) accuracy [17–20].

2 CMS detector

The central feature of the CMS apparatus is a superconducting solenoid of 6 m internal diameter, providing a magnetic field of 3.8 T. Within the superconducting solenoid volume are a silicon pixel and strip tracker, a lead tungstate crystal electromagnetic calorimeter (ECAL), and a brass and scintillator hadron calorimeter (HCAL), each composed of a barrel and two endcap sections. Forward calorimeters extend the pseudorapidity coverage provided by the barrel and endcap detectors. Muons are measured in gas-ionization detectors embedded in the steel flux-return yoke outside the solenoid. A more detailed description of the CMS detector, together with a definition of the coordinate system used and the relevant kinematic variables, can be found in [21].

3 Event simulation

Monte Carlo event generators, interfaced with a detailed detector simulation, are used to assess effects such as reconstruction and selection efficiencies and detector resolutions. The CMS detector response is simulated using GEANT4 (v. 9.4) [22].

The $\mathrm{t\bar{t}}$ process is modelled at NLO using the POWHEG (v. 2) [12, 14] (henceforth referred to as POWHEG V2) event generator with the NNPDF3.0 [23] parton distribution functions (PDF). The generated events are subsequently processed with PYTHIA (v. 8.2) [11] with the CUETP8M1 tune [24, 25] (referred to as PYTHIA8) for parton showering and hadronization.

Predictions for the $\mathrm{t\bar{t}}$ differential cross section are also obtained from alternative generator setups. The MG5_aMC@NLO (v. 2.2.2) [10] event generator is used to simulate two samples of $\mathrm{t\bar{t}}$ production, which are further interfaced with PYTHIA8 for parton showering and hadronization. In one of them (referred to as MG5_aMC@NLO + PYTHIA8 [FxFx]), events are generated with up to two extra partons at the Matrix Element (ME) level at NLO accuracy and are interfaced to MADSPIN [26] to model the decays of the top quarks. The matching of the ME-level partons to parton showers is performed using the FxFx [27] prescription, and the proton structure is described by the NNPDF3.0 PDF set. In the other sample (referred to as MG5_aMC@NLO + PYTHIA8 [MLM]), events are generated with up to three additional partons at LO accuracy at the ME level. The MLM [28] prescription is used for matching of ME-level partons to parton showers, and the PDF set NNPDF2.3 [23] is used. A sample of $\mathrm{t\bar{t}}$ events generated with POWHEG V2 and interfaced with HERWIG++ (v. 2.7.1) [16] with the EE5C tune [29] is used to determine an uncertainty arising from the modelling of the parton shower and hadronization (cf. Section 5). In all samples the value of the top quark mass is assumed to be $m_{\mathrm{t}} = 172.5\,\mathrm{GeV}$.

The main background contributions originate from Z/γ^* bosons produced with additional jets (Z+jets), single top quarks produced in association with a W boson (tW), W boson production with additional jets (W+jets), diboson (WW, WZ, and ZZ) events, and the production of a $\mathrm{t\bar{t}}$ pair in association with a Z or a W boson ($\mathrm{t\bar{t}}$+Z/W). The W+jets, Z+jets, and $\mathrm{t\bar{t}}$+Z/W samples are simulated with MG5_aMC@NLO. POWHEG (v. 1) [13, 15] is used for single top quark production, while PYTHIA8 is used to simulate diboson events. Parton showering and hadronization are also simulated with PYTHIA8 in all the background samples.

For comparison with the measured distributions, the events in the simulated samples are normalized according to their cross sections and an integrated luminosity of 2.2 fb^{-1}. The cross sections are taken from NNLO (W+jets and Z+jets), approximate NNLO (single top quark tW channel [30]), and NLO (diboson [31], $\mathrm{t\bar{t}}$+Z/W [32]) calculations. Correction factors (referred to as scale factors) accounting for the imperfect modelling of the detector response described in Sections 4 and 5 are applied where necessary to improve the description of the data by the simulation.

The $\mathrm{t\bar{t}}$ simulation is normalized to the NNLO+NNLL calculation [33–38], performed with the TOP++2.0 program [39]. The PDF and α_S uncertainties in this calculation are estimated using the PDF4LHC prescription [40, 41] with the MSTW2008nnlo68cl [42], CT10nnlo [43, 44], and NNPDF2.3 [45] PDF sets, and are added in quadrature to the scale uncertainty to obtain a $\mathrm{t\bar{t}}$ production cross section of $831.8\,^{+19.8}_{-29.2}\,(\mathrm{scale}) \pm 35.1(\mathrm{PDF} + \alpha_s)\,\mathrm{pb}$ assuming a top quark mass value of 172.5 GeV. Since normalized differential $\mathrm{t\bar{t}}$ cross sections are measured in this analysis, the normalization of the $\mathrm{t\bar{t}}$ sample is used only to predict the number of $\mathrm{t\bar{t}}$ events in the figures in Section 4 and has no impact on the final results.

4 Event selection

The event selection is similar to that described in [6], and is based on the decay topology where both top quarks decay into a W boson and a b quark, and each of the two W bosons decays into a muon or an electron and a neutrino.

At trigger level, events are required to contain two leptons fulfilling transverse momentum (p_T) thresholds and isolation criteria. The events are subsequently selected offline if they contain two isolated leptons of opposite electric charge and at least two jets. At least one of the jets is required to be identified as a b jet (b-tagged). The events are reconstructed using a particle-flow technique [46, 47], which combines signals from all sub-detectors to enhance the reconstruction performance by identifying individual particle candidates in pp collisions. Charged hadrons from pileup events, i.e. those originating from a vertex other than the one of the hard interaction, are subtracted on an event-by-event basis. Subsequently, the four-vectors of the jets are corrected for the remaining contribution from pileup [48].

The electron candidates are required to have $p_T > 20\,\text{GeV}$ and pseudorapidity $|\eta| < 2.4$, as reconstructed from a combination of the track momentum at the main interaction vertex and the corresponding energy deposition in the ECAL. A relative isolation criterion $I_{\text{rel}} < 0.07$ is required, where I_{rel} is defined as the sum of the p_T of all neutral and charged reconstructed particle candidates inside a cone around the electron in $\eta - \phi$ space of $\Delta R \equiv \sqrt{(\Delta\eta)^2 + (\Delta\phi)^2} < 0.3$, divided by the p_T of the electron. In addition, electrons from identified photon conversions are rejected. Muon candidates are reconstructed using the track information from the silicon tracker and the muon system. They are required to have $p_T > 20\,\text{GeV}$ and $|\eta| < 2.4$. Isolated muon candidates are selected if they fulfill $I_{\text{rel}} < 0.15$ within a cone of $\Delta R < 0.4$ around the muon.

Jets are reconstructed by clustering the particle-flow candidates using the anti-k_t clustering algorithm with a distance parameter of 0.4 [49, 50]. Jets are selected if they have $p_T > 30\,\text{GeV}$ and $|\eta| < 2.4$. A jet-lepton cleaning procedure is applied, which excludes jets overlapping with fully selected leptons if $\Delta R(\text{jet}, \text{lepton}) < 0.4$. Jets originating from b quarks (b-jets) are identified by combining secondary vertices and track-based lifetime information in an algorithm that provides a b-jet efficiency of $\approx$ 82–88% and a probability to misidentify light-flavour jets as b jets of $\approx$ 10% [51].

The missing transverse momentum vector $\vec{p}_T^{\,\text{miss}}$ is defined as the projection on the plane perpendicular to the beams of the negative vector sum of the momenta of all reconstructed particles in an event. Its magnitude is referred to as E_T^{miss}.

Events with an invariant mass of the lepton pair ($m_{\ell\ell}$) smaller than 20 GeV are removed in order to suppress events from heavy-flavour resonance decays and low-mass Drell-Yan processes. Backgrounds from Z+jets processes in the $\mu^+\mu^-$ and e^+e^- channels are further suppressed by requiring $|m_Z - m_{\ell\ell}| > 15\,\text{GeV}$ and E_T^{miss} to be larger than 40 GeV.

Only $t\bar{t}$ events with two leptons that do not originate from the decays of tau leptons are considered as signal with all other $t\bar{t}$ events are regarded as background. The background contribution from Z+jets events, which is large in the e^+e^- and $\mu^+\mu^-$ channels, is determined from data [3, 9]. The Z+jets normalization is determined by extrapolating the number of data events observed in a control region where $m_{\ell\ell}$ is close to m_Z to the signal region via a factor derived from simulation. A correction to account for non-Z+jets backgrounds in the control region is derived from the $\mu^\pm e^\mp$ channel. Other sources of background such as tW, diboson, $t\bar{t}$+Z/W, misidentified leptons, and leptons within jets are estimated from simulation.

In Fig. 1, distributions of the kinematics and multiplicities of the jets, b-jets and leptons in the selected events in data and simulation are shown. The data are generally well described by the simulation.

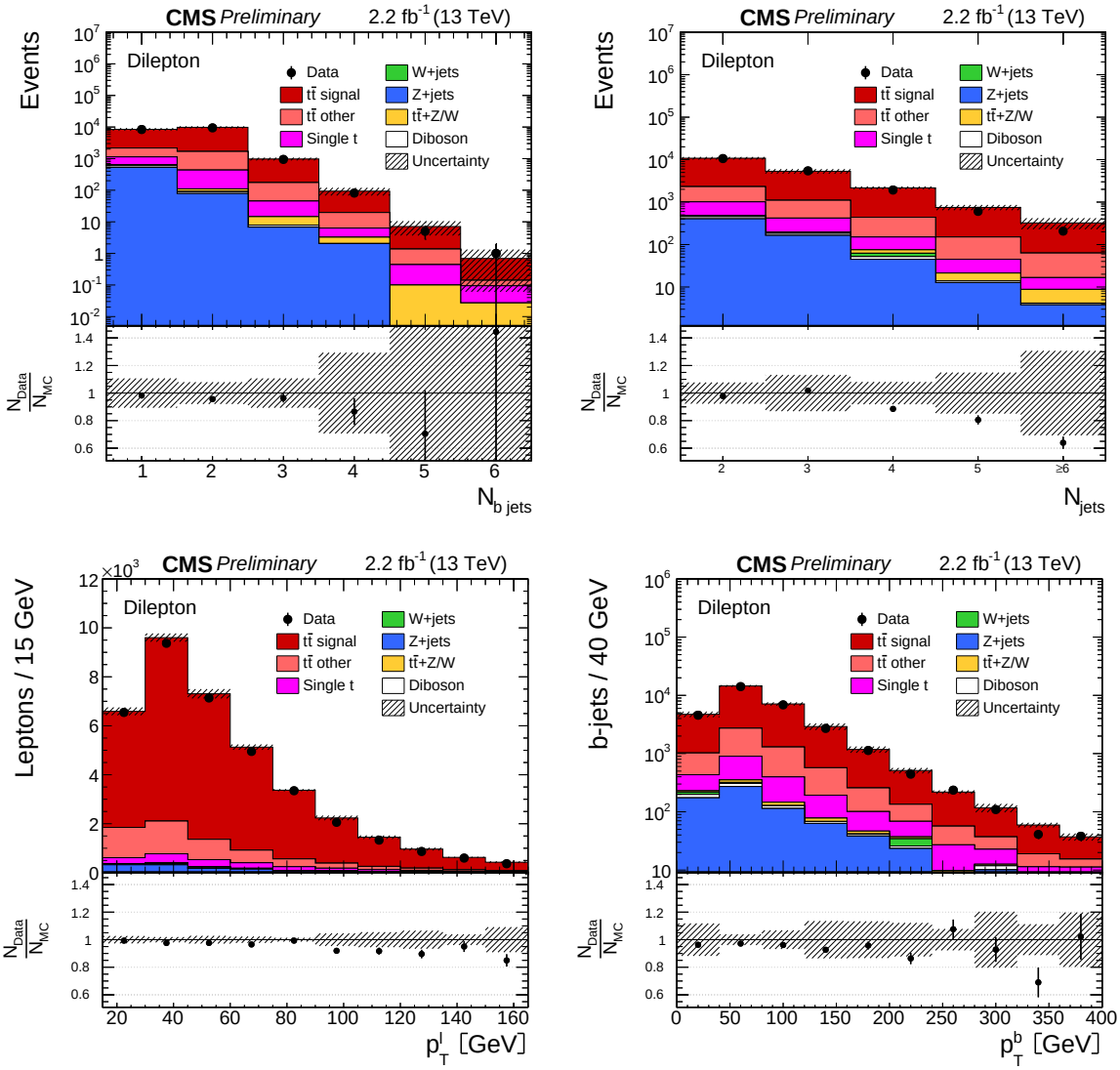

Figure 1: Distributions of the multiplicity of b-jets (top left), the multiplicity of jets (top right), the p_{T} of the selected isolated leptons (bottom left) and the p_{T} of the reconstructed jets (bottom right) are shown. The hatched regions correspond to the systematic shape uncertainties for the signal and backgrounds (cf. Section 5). The lower part of each plot shows the ratio of data to the predictions.

The kinematics of the top quarks are deduced by assigning the final-state objects to the top quark decay products via a kinematic reconstruction algorithm [3, 6]. The algorithm examines all jet-lepton combinations and estimates the kinematics of the top quarks by solving a system of equations while imposing the following constraints: $E_{\mathrm{T}}^{\mathrm{miss}}$ is assumed to originate solely from the two neutrinos; the mass of the reconstructed W boson must equal 80.4 GeV [52]; and the masses of the reconstructed top quarks must equal 172.5 GeV. Effects of detector resolution are accounted for by randomly smearing the measured energies and directions of the reconstructed lepton and b jet candidates by their resolutions. For a given smearing, the solution

of equations for the neutrino momenta yielding the smallest invariant mass of the $\mathrm{t\bar{t}}$ system is chosen. For each solution, a weight is calculated based on the expected true invariant mass spectrum of the lepton and b jet from top quark decays. The weights are summed over 100 reconstruction attempts, and the kinematics of the top quark and antiquark are calculated as a weighted average. Finally, the two jet and lepton-jet assignments that yield the maximum sum of weights are used. Combinations with two b-tagged jets are preferred to using single b-tagged jets. The efficiency of the kinematic reconstruction, defined as the number of events in simulation where a solution is found divided by the total number of selected $\mathrm{t\bar{t}}$ events, is about 90%. Events with no valid solution for the neutrino momenta are excluded from further analysis. The performance in data and simulation is similar for all measured observables.

After applying the full event selection and the kinematic reconstruction of the $\mathrm{t\bar{t}}$ system, 10 257 events are observed in the $\mu^{\pm}\mathrm{e}^{\mp}$ channel, 4 040 events in the $\mu^{+}\mu^{-}$ channel, and 2 636 events in the $\mathrm{e}^{+}\mathrm{e}^{-}$ channel. In all decay channels combined, the signal contribution to the final event sample is 80.6%. The remaining events contain 13.0% $\mathrm{t\bar{t}}$ decays other than the dilepton channels, including $\mathrm{t\bar{t}}$ decays into τ leptons originating from the primary interaction, 3.4% single top tW events, 2.3% Z+jets events, and negligible fractions of W+jets, diboson, and $\mathrm{t\bar{t}}$+Z/W events.

The distributions of the top quark or antiquark and $\mathrm{t\bar{t}}$ kinematic observables ($p_{\mathrm{T}}^{\mathrm{t}}$, y_{t}, $p_{\mathrm{T}}^{\mathrm{t\bar{t}}}$, $y_{\mathrm{t\bar{t}}}$, and $m_{\mathrm{t\bar{t}}}$) are presented in Fig. 2. In general, the data are well described by the simulation within the experimental uncertainties. Good agreement is also observed for the three decay channels.

5 Systematic uncertainties

Different sources of systematic uncertatinties on the measurement are considered arising from detector effects and from theoretical assumptions.

Each systematic uncertainty is investigated separately, and determined individually in each bin of the measurement, by a variation of the corresponding uncertainty source by $\pm$ 1 standard deviation following the procedure described in [3, 6]. For each variation, the measured normalized differential cross section is recalculated, and the difference of the varied result to the nominal one in each bin is taken as the systematic uncertainty. The overall uncertainty on the measurement is derived by adding the individual contributions in quadrature.

Lepton trigger efficiencies are measured using triggers that are only weakly correlated to the dilepton triggers used in the analysis [9]. A dependence on η of a few percent is observed and scale factors are derived. The lepton identification and isolation uncertainties are determined using the "tag-and-probe" method [9, 53] with Z boson event samples, and are found to be described very well by the simulation for both electrons and muons.

The uncertainty arising from the jet energy scale (JES) is determined by the varying the jet energy in bins of p_{T} and η [54]. The uncertainty from the jet energy resolution (JER) is determined by the variation of the simulated JER by $\pm 1\sigma$ in different η regions [54].

The uncertainty on the b-tagging efficiency is determined by dividing the b-jet distributions for p_{T} and η at their median to form two bins. The b-tagging scale factors for the b jets in the first bin are scaled up by half of the uncertainties quoted in [55], while those in the second bin are scaled down and vice versa, so that a maximum variation on the shape of the distribution is obtained and the difference between the scale factors in the two bins reflects the full uncertainty. The variations are performed separately for the p_{T} and η distributions, and independently for heavy-flavour (b and c) and light (s, u, d, and gluon) jets, assuming that they are

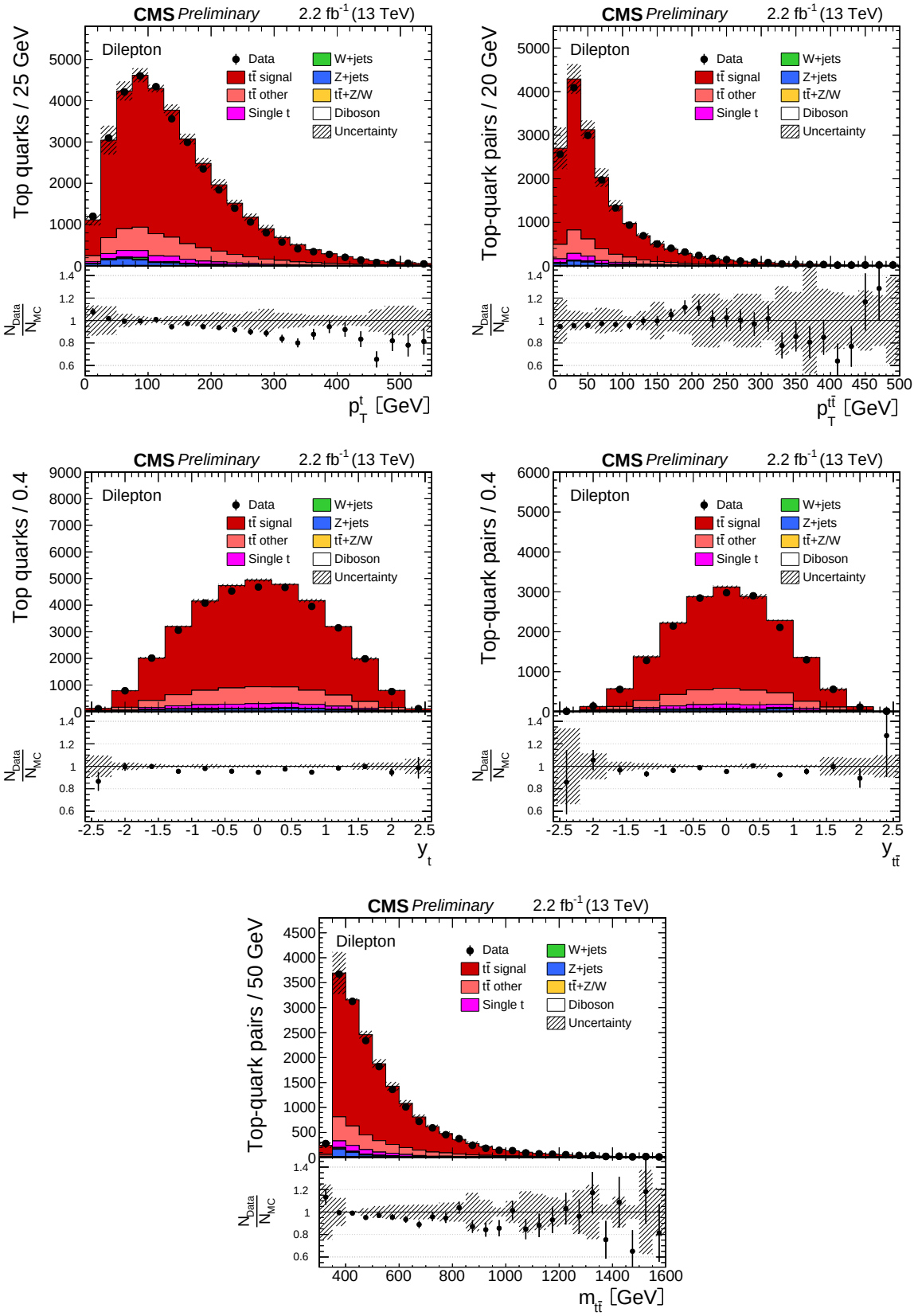

Figure 2: Distributions of the p_T (top), the rapidities (middle), and the invariant mass of the $t\bar{t}$ system (bottom) for the reconstructed top quark (left) and $t\bar{t}$ system (right) are shown. The hatched regions correspond to the shape uncertainties for the signal and backgrounds (cf. Section 5). The lower part of each plot shows the ratio of data to the predictions.

all uncorrelated.

The normalizations of all backgrounds, including the contribution from Z+jets, are varied up and down by$\pm$30% [6, 9].

The kinematic reconstruction of the top quarks is generally found to be well described by the simulation. The uncertainty from the modelling of the number of pileup events is obtained by changing the inelastic proton-proton cross section assumed in the simulation by $\pm$5%.

The uncertainty arising from the missing higher-order terms in the simulation of the $\mathrm{t\bar{t}}$ process at ME level is assessed by variation of the renormalization and factorization scales in the POWHEG V2 simulation up and down by factors of two with respect to the nominal values. In the POWHEG V2 sample, the nominal scales are defined as $m_{\mathrm{t}}^2 + p_{\mathrm{T,t}}^2$, where $p_{\mathrm{T,t}}^2$ denotes the p_{T} of the top quark in the $\mathrm{t\bar{t}}$ rest frame. In addition, the renormalization and factorization scales are varied in parton shower simulation performed by PYTHIA8.

The dependence of the measurement on the assumed top quark mass is estimated from dedicated POWHEG V2 samples in which the top quark mass is varied by $\pm$ 1 GeV with respect to the value used for the default simulation.

The uncertainty due to the hadronization and parton showering model is estimated by comparing samples simulated with POWHEG V2 using PYTHIA8 and HERWIG++ for hadronization. In addition, the flavor-dependent hadronization uncertainty is part of the JES uncertainty and comes from differences in the energy response for different jet flavours and flavour mixtures. It originates in differences between the Lund fragmentation model (PYTHIA8) and cluster fragmentation (HERWIG++), and is evaluated for each jet flavour independently.

The uncertainty on the choice of the generator to model the $\mathrm{t\bar{t}}$ process at ME level is evaluated by comparing samples generated with POWHEG V2 and MG5_aMC@NLO, both interfaced to PYTHIA8.

The effect of the uncertainty from the choice of PDF is assessed by reweighting the sample of simulated $\mathrm{t\bar{t}}$ signal events according to the prescription provided for the NNPDF3.0 PDF set [23].

The overall uncertainty on the measurement ranges from 3$-$30%, depending on the observable and the bin.

6 Normalized differential cross section

For a given variable, X, the normalized differential $\mathrm{t\bar{t}}$ cross section $1/\sigma \cdot \mathrm{d}\sigma/\mathrm{d}X$ is determined via the relation [3, 6]:

$$\frac{1}{\sigma}\frac{\mathrm{d}\sigma_i}{\mathrm{d}X} = \frac{1}{\sigma}\frac{x_i}{\Delta_i^X} \tag{1}$$

where x_i represents the number of signal events observed in data after background subtraction and corrected for detector efficiencies, acceptances, and migrations, and Δ_i^X is the bin width. The normalized differential cross section is obtained by dividing this quantity by the measured total cross section σ in the same phase space, which is evaluated by integrating over all bins for each observable X. The contribution to the background from other $\mathrm{t\bar{t}}$ decays is taken into account, after subtracting all other background components, by correcting the number of signal events in data using the expected signal fraction. The expected signal fraction is defined as the

ratio of the number of selected $\mathrm{t\bar{t}}$ signal events to the total number of selected $\mathrm{t\bar{t}}$ events (i.e. signal and all other $\mathrm{t\bar{t}}$ events) in simulation. This procedure avoids the dependence on the total inclusive $\mathrm{t\bar{t}}$ cross section used in the normalization of the simulated signal sample.

Effects from trigger and detector efficiencies and resolutions leading to the migration of events across bin boundaries and statistical correlations between bins, are accounted for by using a regularized unfolding method [3, 6, 56, 57]. For each measured distribution, a response matrix that accounts for migrations and efficiencies is calculated from the simulated POWHEG V2 $\mathrm{t\bar{t}}$ signal sample. The generalized inverse of the response matrix is used to obtain the unfolded distribution from the measured distribution by applying a χ^2 technique. To avoid non-physical fluctuations, a regularization prescription is applied. The regularization level is determined individually for each distribution using the averaged global correlation method [58].

To keep the bin-to-bin migrations small, the width of the bins of the measurement are chosen according to their purity (sensitive to migrations into the bin) and stability (sensitive to migrations out of the bin). In this analysis, the purity and stability of the bins are typically 50%.

The unfolding is performed separately for each decay channel. The results from the individual channels are found to be consistent with each other and the final result is obtained from their combination. For every systematic variation the full analysis, including the combination, is repeated, and the difference with respect to the nominal value is taken as the systematic uncertainty. This way, systematic correlations between the three decay channels are taken into account. Due to the normalization, those systematic uncertainties that are correlated across all bins of the measurement and only affect the normalization, cancel out.

The normalized differential cross section as a function of the jet multiplicity is determined at the particle level, where the physics objects are defined as follows [6]. Leptons from the W boson decays are defined at the ME level. A jet is defined at the particle level by applying the anti-$\mathrm{k_T}$ clustering algorithm with distance parameter of $R = 0.4$ [49] to all stable particles, excluding both neutrinos and prompt electrons and muons from W boson decays. A jet is defined as a b-jet if it has at least one B hadron associated with it, following the procedure from [4]. To perform the matching between B hadrons and jets, the B hadron momentum is scaled down to a negligible value and included in the jet clustering (so-called ghost matching [59]). In order to avoid the modelling uncertainties introduced by an extrapolation to phase space regions not experimentally accessible, the cross section for the measured jet multiplicity is presented in a fiducial phase space where the leptons have $|\eta_\ell| < 2.4$ and $p_\mathrm{T}^\ell > 20\,\mathrm{GeV}$, and the jets (including both b-jets from the top quark decays) lie within the range $|\eta| < 2.4$ and $p_\mathrm{T} > 30\,\mathrm{GeV}$.

In addition, the top quark and $\mathrm{t\bar{t}}$-system observables are defined at a level before the top quark decay and after QCD radiation which we refer to as the parton level. Parton level results are extrapolated to the full phase space using the POWHEG V2 + PYTHIA8 $\mathrm{t\bar{t}}$ simulation and compared to recent high-order QCD calculations.

The distribution of the jet multiplicity with p_T thresholds above 30 GeV is shown in Fig. 3. The data are compared to the predictions from POWHEG V2 + PYTHIA8, MG5_aMC@NLO + PYTHIA8 [FxFx], MG5_aMC@NLO + PYTHIA8 [MLM], and POWHEG V2 + HERWIG++. The data are not well described by any of the considered predictions for multiplicities > 4, which correspond to the region in which the effect of the parton shower is expected to dominate the prediction.

The normalized differential $\mathrm{t\bar{t}}$ cross section as a function of the kinematics of the top quarks and the $\mathrm{t\bar{t}}$ system is presented at parton level and extrapolated to the full phase space using the POWHEG V2 + PYTHIA8 $\mathrm{t\bar{t}}$ simulation. In Figs. 4 to 6 the distributions for the transverse

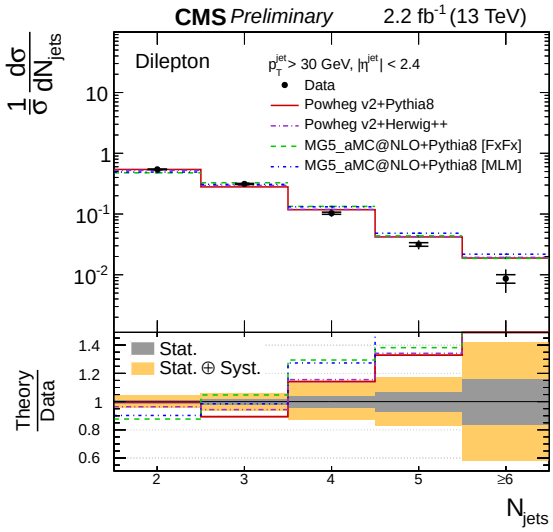

Figure 3: The normalized differential $\mathrm{t\bar{t}}$ production cross section as a function of the jet multiplicity is shown. The inner (outer) error bars indicate the statistical (combined statistical and systematic) uncertainty. The data are compared to predictions from POWHEG V2 + PYTHIA8, MG5_aMC@NLO + PYTHIA8 [FxFx], MG5_aMC@NLO + PYTHIA8 [MLM], and POWHEG V2 + HERWIG++.

momentum $p_{\mathrm{T}}^{\mathrm{t}}$ and the rapidity y_{t} of the top quarks or antiquarks, and the transverse momentum $p_{\mathrm{T}}^{\mathrm{t\bar{t}}}$, rapidity $y_{\mathrm{t\bar{t}}}$, and invariant mass $m_{\mathrm{t\bar{t}}}$ of the $\mathrm{t\bar{t}}$ system are presented. Also shown are predictions from MG5_aMC@NLO interfaced to PYTHIA8, and from POWHEG V2 interfaced to both PYTHIA8 and HERWIG++.

In addition, the parton level results are compared to several QCD calculations that offer beyond-NLO accuracy:

- An approximate next-to-next-to-leading-order (NNLO) calculation [17] (referred to as approx. NNLO) based on QCD threshold expansions beyond the leading logarithmic approximation using the CT14nnlo [60] PDF set. The top quark mass value is assumed to be $m_{\mathrm{t}} = 172.5\,\mathrm{GeV}$, and the factorization and renormalization scales are fixed to the m_{t} value.
- An approximate next-to-next-to-next-to-leading-order calculation [18] (referred to as approx. N^{3}LO) based on the resummation of soft-gluon contributions in the double-differential cross section at next-to-next-to-leading-logarithm (NNLL) accuracy in the moment-space approach. The MSTW2008nnlo PDF set is used and the top quark mass value is $m_{\mathrm{t}} = 172.5\,\mathrm{GeV}$. The renormalization and factorization scales are set to the m_{t} value.
- A full NNLO calculation [19] (referred to as NNLO) using the NNPDF3.0 PDF set, $m_{\mathrm{t}} = 173.3\,\mathrm{GeV}$, and dynamic (i.e., kinematics-dependent) renormalization and factorization scales (m_T for $p_{\mathrm{T}}^{\mathrm{t}}$, where $m_T = \sqrt{m_{\mathrm{t}}^2 + p_{\mathrm{T}}^{\mathrm{t}2}}$, and $H_T/4$ for y_{t}, $p_{\mathrm{T}}^{\mathrm{t\bar{t}}}$, $y_{\mathrm{t\bar{t}}}$, and $m_{\mathrm{t\bar{t}}}$).
- An NLO+NNLL′ prediction [20] (referred to as NLO+NNLL′) that includes the simultaneous resummation of soft and small-mass logarithms to NNLL′ accuracy, matched with both the standard soft-gluon resummation at NNLL accuracy and the fixed-order calculation at NLO accuracy. These corrections are expected to affect the

high-energy tails of the ttbar differential distributions. The calculation is performed using the MTSW2008nnlo PDF set, $m_{\mathrm{t}} = 173.2\,\mathrm{GeV}$, and dynamic renormalization and factorization scales (m_T for $p_{\mathrm{T}}^{\mathrm{t}}$ and $m_{\mathrm{t\bar{t}}}/2$ for $m_{\mathrm{t\bar{t}}}$).

All the calculations include an uncertainty on the change of the cross section due to variation of the renormalization and factorization scales. Moreover, the approx. NNLO calculation also includes uncertainties on the PDF, the choice of α_S, and the uncertainty on the variation of m_{t} by $\pm 1\,\mathrm{GeV}$, which are all added in quadrature to the scale uncertainty.

In general, good agreement is observed between data and all considered predictions within uncertainties. The top quark p_{T} spectrum in data tends to be lower than the Monte Carlo predictions for $p_{\mathrm{T}}^{\mathrm{t}} > 200\,\mathrm{GeV}$, and is better described by POWHEG V2 + HERWIG++. This effect was also observed at 8 TeV by the ATLAS [5] and CMS [3] collaborations. All the considered calculations provide a good description of the data for all $p_{\mathrm{T}}^{\mathrm{t}}$ values within the uncertainty of the measurement. The $m_{\mathrm{t\bar{t}}}$ distribution in data is well described by all predictions in the given range within uncertainties. The shape of the $p_{\mathrm{T}}^{\mathrm{t\bar{t}}}$ spectrum is overall better described by POWHEG V2 + PYTHIA8 and by the NNLO calculation. Both the y_{t} and $y_{\mathrm{t\bar{t}}}$ distributions are well described by all considered predictions given the current precision of the measurement.

7 Summary

Measurements of normalized differential $\mathrm{t\bar{t}}$ production cross sections in pp collisions at $\sqrt{s} = 13\,\mathrm{TeV}$ with the CMS detector are presented. The measurements are performed in the dilepton ($\mathrm{e^+e^-}$, $\mu^+\mu^-$, and $\mu^{\pm}\mathrm{e}^{\mp}$) decay channels. The normalized $\mathrm{t\bar{t}}$ cross section is measured as a function of the jet multiplicity in the event for jet p_{T} thresholds above 30 GeV in the fiducial phase space, and of the p_{T}, rapidity, and invariant mass of the top quarks and $\mathrm{t\bar{t}}$ system in the full phase space. In general, the data are in agreement with the state-of-the-art of standard model QCD predictions for all measured distributions. However, the jet multiplicity in data is not properly described by any of the considered Monte Carlo predictions for high multiplicity values. The top quark p_{T} spectrum in data is found to be softer than the Monte Carlo predictions, and is better described by QCD calculations beyond NLO accuracy. The observed effect is in agreement with the corresponding results from the ATLAS and CMS collaborations at $\sqrt{s} = 7$ and 8 TeV.

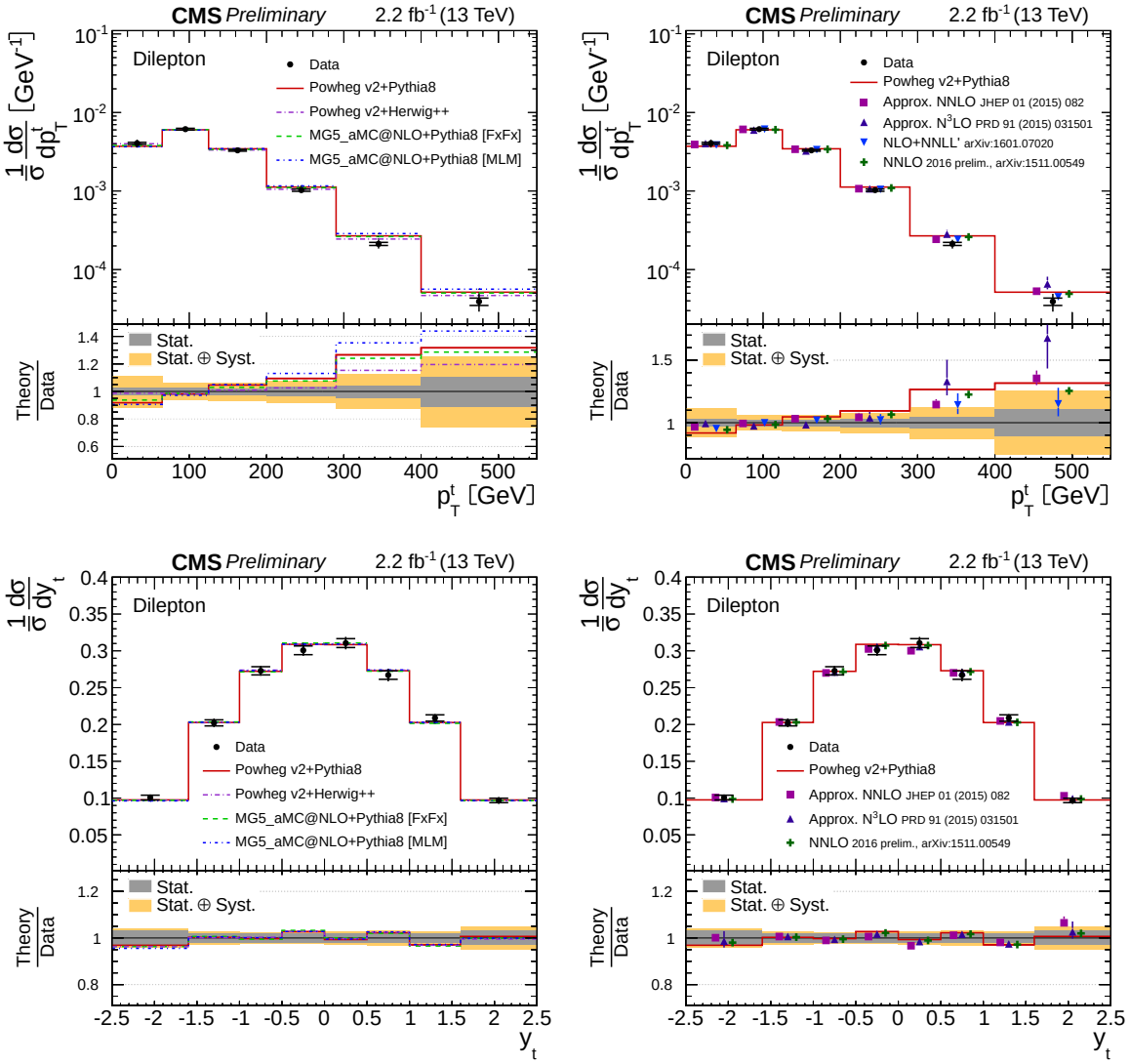

Figure 4: Normalized differential $t\bar{t}$ production cross section as a function of the p_T^t (top) and y_t (bottom) of the top quarks or antiquarks. The inner (outer) error bars indicate the statistical (combined statistical and systematic) uncertainty. The data are compared to predictions from POWHEG V2 + PYTHIA8, MG5_aMC@NLO + PYTHIA8 [FxFx], MG5_aMC@NLO + PYTHIA8 [MLM], and POWHEG V2 + HERWIG++ (left), and to beyond-NLO QCD calculations [17–20] (right), when available.

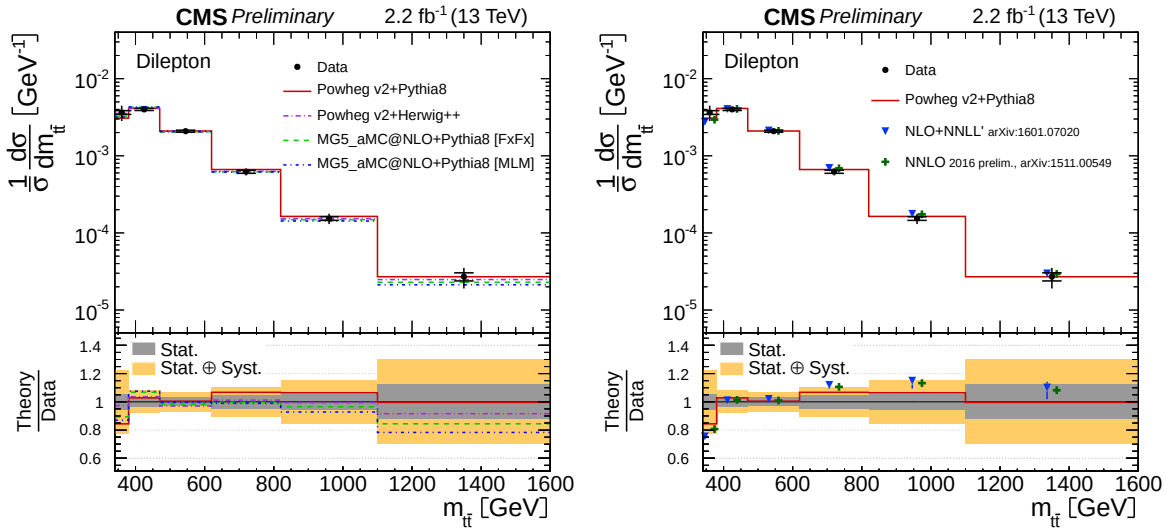

Figure 5: Normalized differential $t\bar{t}$ production cross section as a function of the $m_{t\bar{t}}$ of the top quark pairs. The inner (outer) error bars indicate the statistical (combined statistical and systematic) uncertainty. The data are compared to predictions from POWHEG V2 + PYTHIA8, MG5_aMC@NLO + PYTHIA8 [FxFx], MG5_aMC@NLO + PYTHIA8 [MLM], and POWHEG V2 + HERWIG++ (left), and to beyond-NLO QCD calculations [19, 20] (right).

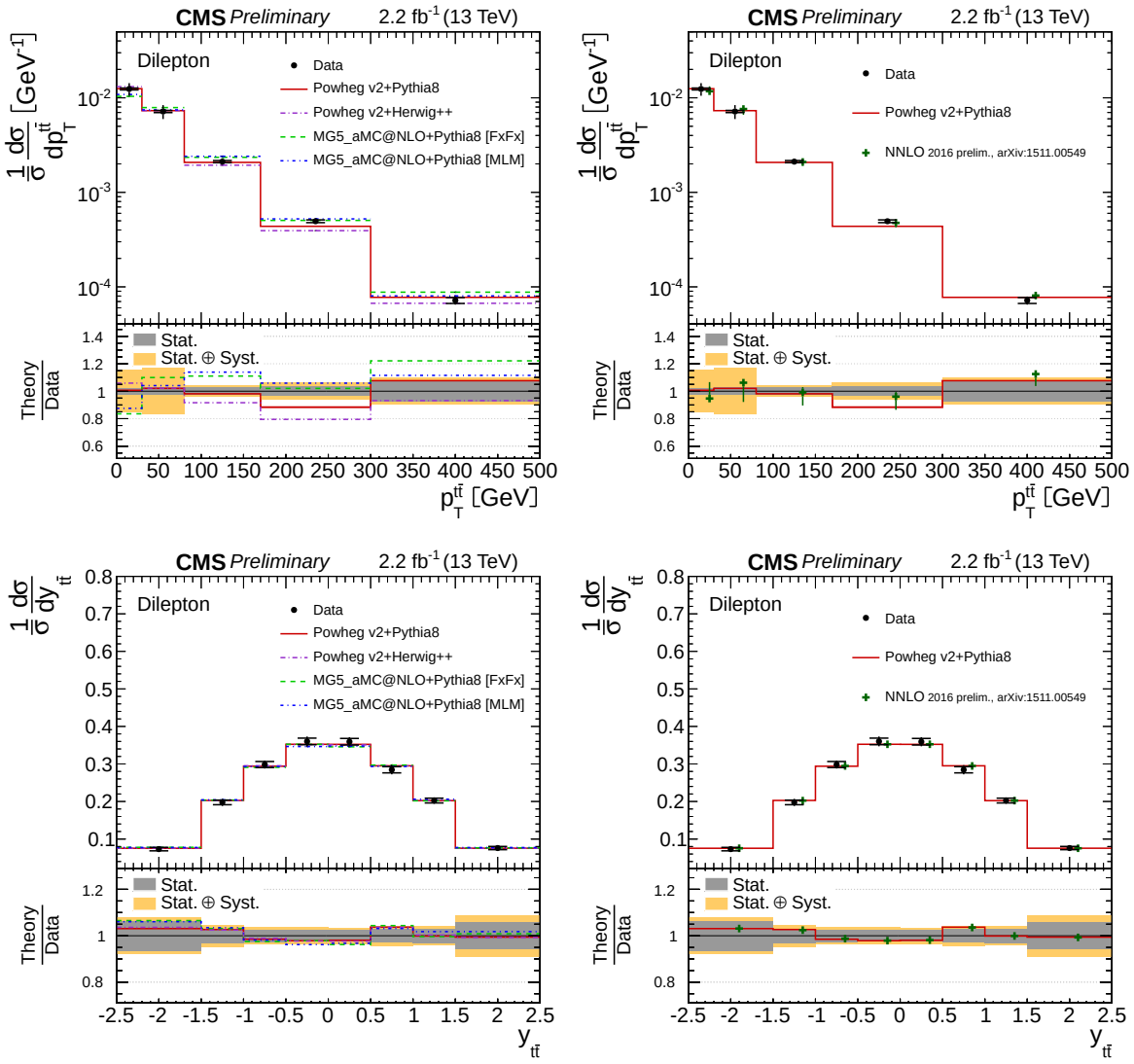

Figure 6: Normalized differential $t\bar{t}$ production cross section as a function of the $p_T^{t\bar{t}}$ (top), $y_{t\bar{t}}$ (bottom) of the top quark pairs. The inner (outer) error bars indicate the statistical (combined statistical and systematic) uncertainty. The data are compared to predictions from POWHEG v2 + PYTHIA8, MG5_aMC@NLO + PYTHIA8 [FxFx], MG5_aMC@NLO + PYTHIA8 [MLM], and POWHEG v2 + HERWIG++ (left), and to beyond-NLO QCD calculations [19] (right).

References

[1] ATLAS Collaboration, "Measurements of top quark pair relative differential cross-sections with ATLAS in pp collisions at $\sqrt{s}$ = 7 TeV", *Eur. Phys. J. C* **73** (2013) 2261, doi:10.1140/epjc/s10052-012-2261-1, arXiv:1207.5644.

[2] CMS Collaboration, "Measurement of differential top-quark pair production cross sections in pp collisions at $\sqrt{s} = 7$ TeV", *Eur. Phys. J. C* **73** (2013) 2339, doi:10.1140/epjc/s10052-013-2339-4, arXiv:1211.2220.

[3] CMS Collaboration, "Measurement of the differential cross section for top quark pair production in pp collisions at $\sqrt{s} = 8$ TeV", *Eur. Phys. J. C* **75** (2015) 542, doi:10.1140/epjc/s10052-015-3709-x, arXiv:1505.04480.

[4] CMS Collaboration, "Measurement of ttbar production with additional jet activity, including b quark jets, in the dilepton channel using pp collisions at $\sqrt{s}$ = 8 TeV", (2015). arXiv:1510.03072. Submitted to Eur. Phys. J. C.

[5] ATLAS Collaboration, "Measurements of top-quark pair differential cross-sections in the lepton+jets channel in pp collisions at $\sqrt{s} = 8$ TeV using the ATLAS detector", (2015). arXiv:1511.04716. Submitted to Eur. Phys. J. C.

[6] CMS Collaboration, "First measurement of the differential cross section for top quark pair production proton-proton collisions at $\sqrt{s}$ = 13 TeV", CMS Physics Analysis Summary CMS-PAS-TOP-15-010, 2015.

[7] CMS Collaboration, "Measurement of the inclusive and differential tt production cross sections in lepton + jets final states at 13 TeV", CMS Physics Analysis Summary CMS-PAS-TOP-15-005, 2015.

[8] CMS Collaboration, "CMS luminosity measurement for the 2015 data taking period", CMS Physics Analysis Summary CMS-PAS-LUM-15-001, 2016.

[9] CMS Collaboration, "Measurement of the top quark pair production cross section in proton-proton collisions at $\sqrt{s}$ = 13 TeV with the CMS detector", *Phys. Rev. Lett.* **116** (2016) 052002, doi:10.1103/PhysRevLett.116.052002, arXiv:arXiv:1510.05302.

[10] J. Alwall et al., "The automated computation of tree-level and next-to-leading order differential cross sections, and their matching to parton shower simulations", *JHEP* **07** (2014) 079, doi:10.1007/JHEP07(2014)079, arXiv:1405.0301.

[11] T. Sjöstrand et al., "An introduction to PYTHIA 8.2", *Comput. Phys. Commun.* **191** (2015) 159, doi:10.1016/j.cpc.2015.01.024, arXiv:1410.3012.

[12] S. Frixione, P. Nason, and C. Oleari, "Matching NLO QCD computations with parton shower simulations: the POWHEG method", *JHEP* **11** (2007) 070, doi:10.1088/1126-6708/2007/11/070, arXiv:0709.2092.

[13] S. Alioli et al., "NLO single-top production matched with shower in POWHEG: s- and t-channel contributions", *JHEP* **09** (2009) 111, doi:10.1088/1126-6708/2009/09/111, arXiv:0907.4076.

[14] S. Alioli et al., "A general framework for implementing NLO calculations in shower Monte Carlo programs: the POWHEG BOX", *JHEP* **06** (2010) 043, doi:10.1007/JHEP06(2010)043, arXiv:1002.2581.

[15] E. Re, "Single-top Wt-channel production matched with parton showers using the POWHEG method", *Eur. Phys. J. C* **71** (2011) 1547, doi:10.1140/epjc/s10052-011-1547-z, arXiv:1009.2450.

[16] M. Bahr et al., "Herwig++ Physics and Manual", *Eur. Phys. J. C* **58** (2008) 639–707, doi:10.1140/epjc/s10052-008-0798-9, arXiv:0803.0883.

[17] M. Guzzi, K. Lipka, and S.-O. Moch, "Top-quark pair production at hadron colliders: differential cross section and phenomenological applications with DiffTop", *JHEP* **01** (2015) 082, doi:10.1007/JHEP01(2015)082, arXiv:1406.0386.

[18] N. Kidonakis, "NNNLO soft-gluon corrections for the top-quark p_{T} and rapidity distributions", *Phys. Rev. D* **91** (2015) 031501, doi:10.1103/PhysRevD.91.031501, arXiv:1411.2633.

[19] M. Czakon, D. Heymes, and A. Mitov, "High-precision differential predictions for top-quark pairs at the LHC", arXiv:1511.00549.

[20] B. D. Pecjak, D. J. Scott, X. Wang, and L. L. Yang, "Resummed differential cross sections for top-quark pairs at the LHC", arXiv:1601.07020.

[21] CMS Collaboration, "The CMS experiment at the CERN LHC", *JINST* **3** (2008) S08004, doi:10.1088/1748-0221/3/08/S08004.

[22] GEANT4 Collaboration, "GEANT4—a simulation toolkit", *Nucl. Instrum. Meth. A* **506** (2003) 250, doi:10.1016/S0168-9002(03)01368-8.

[23] NNPDF Collaboration, "Unbiased global determination of parton distributions and their uncertainties at NNLO and LO", *Nucl. Phys. B* **855** (2012) 153, doi:10.1016/j.nuclphysb.2011.09.024, arXiv:1107.2652.

[24] CMS Collaboration, "Underlying event tunes and double parton scattering", CMS Physics Analysis Summary CMS-PAS-GEN-14-001, 2014.

[25] P. Skands, S. Carrazza, and J. Rojo, "Tuning PYTHIA 8.1: the Monash 2013 Tune", *Eur. Phys. J. C* **74** (2014), no. 8, 3024, doi:10.1140/epjc/s10052-014-3024-y, arXiv:1404.5630.

[26] P. Artoisenet et al., "Automatic spin-entangled decays of heavy resonances in Monte Carlo simulations", *JHEP* **03** (2013) 015, doi:10.1007/JHEP03(2013)015, arXiv:1212.3460.

[27] R. Frederix and S. Frixione, "Merging meets matching in MC@NLO", *JHEP* **12** (2012) 061, doi:10.1007/JHEP12(2012)061, arXiv:1209.6215.

[28] M. L. Mangano, M. Moretti, F. Piccinini, and M. Treccani, "Matching matrix elements and shower evolution for top-quark production in hadronic collisions", *JHEP* **01** (2007) 013, doi:10.1088/1126-6708/2007/01/013, arXiv:hep-ex/0611129.

[29] M. H. Seymour and A. Siodmok, "Constraining MPI models using σ_{eff} and recent Tevatron and LHC Underlying Event data", *JHEP* **10** (2013) 113, doi:10.1007/JHEP10(2013)113, arXiv:1307.5015.

[30] N. Kidonakis, "Two-loop soft anomalous dimensions for single top quark associated production with W^- or H^-", *Phys. Rev. D* **82** (2010) 054018, doi:10.1103/PhysRevD.82.054018, arXiv:hep-ph/1005.4451.

[31] J. M. Campbell, R. K. Ellis, and C. Williams, "Vector boson pair production at the LHC", *JHEP* **07** (2011) 018, doi:10.1007/JHEP07(2011)018, arXiv:1105.0020.

[32] F. Maltoni, D. Pagani, and I. Tsinikos, "Associated production of a top-quark pair with vector bosons at NLO in QCD: impact on $t\bar{t}H$ searches at the LHC", arXiv:1507.05640.

[33] M. Cacciari et al., "Top-pair production at hadron colliders with next-to-next-to-leading logarithmic soft-gluon resummation", *Phys. Lett. B* **710** (2012) 612, arXiv:1111.5869.

[34] P. Baernreuther et al., "Percent Level Precision Physics at the Tevatron: First Genuine NNLO QCD Corrections to $q\bar{q} \to t\bar{t} + X$", *Phys. Rev. Lett.* **109** (2012) 132001, doi:10.1103/PhysRevLett.109.132001, arXiv:1204.5201.

[35] M. Czakon and A. Mitov, "NNLO corrections to top-pair production at hadron colliders: the all-fermionic scattering channels", *JHEP* **12** (2012) 054, arXiv:1207.0236.

[36] M. Czakon and A. Mitov, "NNLO corrections to top-pair production at hadron colliders: the quark-gluon reaction", *JHEP* **01** (2013) 080, arXiv:1210.6832.

[37] M. Beneke et al., "Hadronic top-quark pair production with NNLL threshold resummation", *Nucl. Phys. B* **855** (2012) 695, doi:10.1016/j.nuclphysb.2011.10.021, arXiv:1109.1536.

[38] M. Czakon, P. Fiedler, and A. Mitov, "Total Top-Quark Pair-Production Cross Section at Hadron Colliders Through $O(\alpha_S{}^4)$", *Phys.Rev.Lett.* **110** (2013) 252004, doi:10.1103/PhysRevLett.110.252004, arXiv:1303.6254.

[39] M. Czakon and A. Mitov, "Top++: A Program for the Calculation of the Top-Pair Cross-Section at Hadron Colliders", *Comput.Phys.Commun.* **185** (2014) 2930, doi:10.1016/j.cpc.2014.06.021, arXiv:1112.5675.

[40] S. Alekhin et al., "The PDF4LHC Working Group Interim Report", arXiv:1101.0536.

[41] M. Botje et al., "The PDF4LHC Working Group Interim Recommendations", arXiv:1101.0538.

[42] A. D. Martin, W. J. Stirling, R. S. Thorne, and G. Watt, "Parton distributions for the LHC", *Eur. Phys. J. C* **63** (2009) 189, doi:10.1140/epjc/s10052-009-1072-5, arXiv:0901.0002.

[43] H.-L. Lai et al., "New parton distributions for collider physics", *Phys. Rev. D* **82** (2010) 074024, doi:10.1103/PhysRevD.82.074024, arXiv:1007.2241.

[44] J. Gao et al., "CT10 next-to-next-to-leading order global analysis of QCD", *Phys. Rev. D* **89** (2014) 033009, doi:10.1103/PhysRevD.89.033009, arXiv:1302.6246.

[45] NNPDF Collaboration, "Parton distributions with LHC data", *Nucl. Phys. B* **867** (2013) 244, doi:10.1016/j.nuclphysb.2012.10.003, arXiv:1207.1303.

[46] CMS Collaboration, "Particle–flow event reconstruction in CMS and performance for jets, taus, and $E_{\mathrm{T}}^{\mathrm{miss}}$", CMS Physics Analysis Summary CMS-PAS-PFT-09-001, 2009.

[47] CMS Collaboration, "Commissioning of the particle-flow event reconstruction with the first LHC collisions recorded in the CMS detector", CMS Physics Analysis Summary CMS-PAS-PFT-10-001, 2010.

[48] M. Cacciari, G. P. Salam, and G. Soyez, "The catchment area of jets", *JHEP* **04** (2008) 005, doi:10.1088/1126-6708/2008/04/005, arXiv:0802.1188.

[49] M. Cacciari, G. P. Salam, and G. Soyez, "The anti-k_t jet clustering algorithm", *JHEP* **04** (2008) 063, doi:10.1088/1126-6708/2008/04/063, arXiv:0802.1189.

[50] M. Cacciari, G. P. Salam, and G. Soyez, "FastJet user manual", *Eur. Phys. J. C* **72** (2012) 1896, doi:10.1140/epjc/s10052-012-1896-2, arXiv:1111.6097.

[51] CMS Collaboration, "Identification of b quark jets at the CMS experiment in the LHC Run 2", CMS Physics Analysis Summary CMS-PAS-BTV-15-001, 2016.

[52] Particle Data Group, K. A. Olive et al., "Review of Particle Physics", *Chin. Phys. C* **38** (2014) 090001, doi:10.1088/1674-1137/38/9/090001.

[53] CMS Collaboration, "Measurement of the Drell-Yan cross sections in pp collisions at $\sqrt{s}$ = 7 TeV with the CMS experiment", *JHEP* **10** (2011) 007, doi:10.1007/JHEP10(2011)007, arXiv:1108.0566.

[54] CMS Collaboration, "Determination of jet energy calibration and transverse momentum resolution in CMS", *JINST* **6** (2011) P11002, doi:10.1088/1748-0221/6/11/P11002, arXiv:1107.4277.

[55] CMS Collaboration, "Identification of b-quark jets with the CMS experiment", *JINST* **8** (2013) P04013, doi:10.1088/1748-0221/8/04/P04013, arXiv:1211.4462.

[56] A. Hoecker and V. Kartvelishvili, "SVD Approach to Data Unfolding", *Nucl.Instrum.Meth.* **A372** (1996) 469–481, doi:10.1016/0168-9002(95)01478-0, arXiv:hep-ph/9509307v2.

[57] V. Blobel, "An unfolding method for high energy physics experiments", arXiv:0208022.

[58] F. James, "Statistical methods in experimental physics". World Scientific, second edition, 2006.

[59] M. Cacciari, G. P. Salam, and G. Soyez, "The catchment area of jets", *JHEP* **04** (2008) 005, doi:10.1088/1126-6708/2008/04/005, arXiv:0802.1188.

[60] S. Dulat et al., "New parton distribution functions from a global analysis of quantum chromodynamics", *Phys. Rev.* **D93** (2016), no. 3, 033006, doi:10.1103/PhysRevD.93.033006, arXiv:1506.07443.